NANO · MICRO small
www.small-journal.com

Disposable 3D GNAs/AuNPs DNA-Circuit Strip for miRNAs Dynamic Quantification

Jing Bao, Xiaopei Qiu, Huisi Yang, Wenqiang Lu, Mei Yang, Wei Gu, Lixiang Wu, Danqun Huo, Yang Luo,* and Changjun Hou**

Real-time quantitative monitoring of miRNAs plays an essential role in diagnosis and therapeutics. Herein, a DSN-coupled graphene nanoarray/gold nanoparticles (GNAs/AuNPs) carbon paper (CP) electrode for the dynamic, sensitive, and real-time analysis of miRNAs is reported. GNAs are vertically grown on the conductive CP by radio frequency plasma enhanced chemical vapor deposition, and AuNPs are electrodeposited on CP/GNAs to build a 3D ultrasensitive sensing interface with large specific surface area, good conductivity and biocompatibility. The dynamic quantitative monitoring of microRNA-21 (miR-21) is realized by cyclic voltammetry with a series of different concentrations within 16 min, and this 3D GNAs/AuNPs DNA-circuit strip shows good performance for the simultaneous detection of miR-21 and miR-155, and the detection limits are as low as 21.4 and 30.3 am, respectively. Moreover, comparable detection results are achieved for clinical samples between the proposed sensor and qRT-PCR, suggesting the reliability of the constructed sensor. This ultrasensitive sensing and disposable DNA-circuit strip with 3D structure can efficiently shorten the diffusion distance between reactive biomolecules and the sensing interface, enhance the hybridization of probes and improve the sensitivity of the biosensor, holding great promise for the rapid, quantitative and dynamic monitoring of multiple low concentrations of biomolecules in point-of-care clinical analysis.

1. Introduction

MicroRNAs (miRNAs) are representative disease-associated indicators frequently analyzed in fields involving biology, toxicology, and medical sciences.[1–3] Particularly, abnormal expression of miRNAs (upregulated or downregulated) is tightly contacted with the occurrence and development of cancer, which are regarded as promising biomarkers for the prognosis, diagnosis, and treatment of different cancers.[4,5] Continuously and dynamically monitoring miRNAs regulation process is particularly meaningful in achieving more precise information with less time and reagent consumption. Unfortunately, the miRNAs abundance circulating in the peripheral system is extremely low and the short lengths of mature miRNAs thwarts the design of affordable polymerase chain reaction (PCR) primers directly,[6] thus it still remains a huge challenge for sensitive and quick quantitation of trace circulating miRNAs. Classic techniques for miRNA expression analysis like Northern blotting,[7] microarray,[8] qRT-PCR[9] have been

Dr. J. Bao, H. Yang, Prof. M. Yang, Prof. W. Gu, Prof. D. Huo, Prof. C. Hou
Key Laboratory for Biorheological Science and Technology
of Ministry of Education
State and Local Joint Engineering Laboratory for Vascular Implants
Bioengineering College of Chongqing University
Chongqing 400044, China
E-mail: huodq@cqu.edu.cn; houcj@cqu.edu.cn

X. Qiu
Department of Clinical Laboratory
Southwest Hospital
Third Military Medical University (Army Medical University)
Chongqing 400038, China

Prof. W. Lu
Chongqing Key Laboratory of Multi-Scale Manufacturing Technology
Chongqing Institute of Green and Intelligent Technology
Chinese Academy of Sciences
Chongqing 400714, China

The ORCID identification number(s) for the author(s) of this article can be found under https://doi.org/10.1002/smll.202001416.

DOI: 10.1002/smll.202001416

Prof. W. Gu, Prof. Y. Luo
Center of Smart Laboratory and Molecular Medicine
Medical School of Chongqing University
Chongqing 400044, China
E-mail: luoy@cqu.edu.cn

Prof. L. Wu
Department of Clinical Laboratory Chongqing University Cancer
Hospital and Chongqing Cancer Institute and Chongqing Cancer Hospital
No. 181 Han Yu Road, Chongqing 400030, China

Prof. C. Hou
Chongqing Key Laboratory of Bio-perception and Intelligent
Information Processing
School of Microelectronics and Communication Engineering
Chongqing University
Chongqing 400044, China

Prof. Y. Luo
Nuclear Medicine and Molecular Imaging Key Laboratory
of Sichuan Province
Department of Nuclear Medicine
The Affiliated Hospital
Southwest Medical University
Luzhou, Sichuan 646000, China

criticized for their being tedious and time consuming, and always requiring professional operators. More importantly, performing these above-mentioned assays requires discontinuous steps so that only endpoint data could be provided.

In the attempts to provide real-time monitoring miRNAs quantity process, our group had constructed a surface plasmon resonance (SPR)-based strategy that employed duplex-specific nuclease (DSN) for signal amplification. DSN is a particular robot due to its inherent and specific preference for only hydrolyzing DNA in DNA-RNA heteroduplexes rather than in single-stranded (ss) DNA or RNA.[10,11] Although the above method can achieve monitoring dynamic behavior of miRNA detection, it is limited by the number of random rGO SPR chip-coated probes, and its sensitivity cannot fully meet the clinical needs. Considering the linear simplification characteristic of DSN enzyme, the sensitivity of any DSN-based approach is largely limited by the coated DNA probe amounts and the transducing strategies.[12–14] Compared with SPR-based strategy, several highly sensitive detection platforms integrating fluorescence,[15] surface-enhanced Raman scattering (SERS),[3] and electrochemical methods[16] received a lot of attention for the detection of miRNA. Among them, electrochemical method has demonstrated higher sensitivity because the electrode surface could be conveniently structured and functionalized to greatly increase the immobilization of probes and enhance the detection efficiency.[17–19]

As we all know, a number of functionalized nanomaterial-based electroanalytical strategies with various nanostructures have been developed to improve the sensitivity and performance of the electrochemical biosensor for the monitoring of low abundant biomarkers in real samples, including carbon nanostructures (e.g., graphene and CNTs), metal and metal oxide nanoparticles, quantum dots, and some composite nanomaterials.[20–23] Unfortunately, bioelectrodes based on these materials still suffer some inadequacies, such as the agglomeration of nanomaterials on the conventional supporting substrates (glassy carbon electrode [GCE] and gold electrodes [AuE]) reduces the active surface area. Additionally, expensive adhesives (such as nafion or chitosan) and complex steps are needed to improve the stability and prevent the leaking and rupturing of adhesive materials from the modified electrode.[24] An ideal bioelectrode should have good biocompatibility, controllable morphology, a uniform dispersion of the active sites, and good stability, together with high conductivity to ensure efficient electron transportation. Therefore, the in situ preparation of uniformly controllable material on an electrode with good performance is highly preferred.

Owing to the excellent flexibility, environmental friendliness, and electrical conductivity, carbon paper (CP) is expected to be a good conductivity, high chemical stability, low-cost material as an electrode substrate.[25–27] Graphene, a 2D carbon network with extraordinary properties, is considered as a promising candidate of electrode material due to its high specific surface area, excellent electrical conductivity, negligible capacitive current, porous network structure, and good biocompatible properties.[28,29] Till date, various strategies for producing graphene layers have been investigated, such as chemical and mechanical exfoliation,[30,31] chemical vapor deposition (CVD),[32] epitaxial growth on a crystal substrate,[33] etc. In particular, plasma-enhanced chemical vapor deposition (PECVD) is a superior direct growth approach of graphene on various conductive substrates at low temperature and low pressure without the presence of any metal catalyst and post-transfer treatment, which efficiently avoids the complex transfer processes and transfer-induced defects of graphene.[34] In addition, the high electric field aligned perpendicular to the surface conduces the unique 3D structure of the vertically oriented graphene (VG), which can overcome the shortcomings of powdered graphene, and it also has unique advantages such as rich electrolyte diffusion channels, good stability, and strong repeatability.[35] Notably, the 3D morphology and microstructure of vertically oriented graphene (VG) can be adjusted by the gas proportion of H_2 and CH_4, plasma power, growth temperature, and growth time, which ensures the stability of the sensor, and facilitates large scale and applied in the point-of-care clinical analysis.[36]

Herein, we develop a 3D GNAs/AuNPs DNA-circuit strip for continuous monitoring determination of miRNAs. Notably, the behavior of miRNA-DNA hybridization and DSN cleavage have been dynamically monitored using this proposed assay. The sensitive, quantitative, and controllable recognition of miRNA was achieved by integrating the advantages of DSN-mediated recycling amplification and the high target capture capability of this disposable, controllable, and flexible DNA-circuit strip in coating oligonucleotide probes as well as electrochemical biosensor-associated real-time monitoring. Thus, the proposed controllable 3D GNAs/AuNPs DNA-circuit strip exhibits great potential for biological detection and clinical diagnosis.

2. Experimental Section

2.1. Reagents and Materials

HPLC-purified SH-labeled DNA probes and miRNAs listed in **Table 1** were synthesized by Shanghai Sangon Biological Engineering Technology & Services Co., Ltd. (Shanghai, China). A DSN kit containing 100 U DSN and 10× DSN master buffer (50 mM Tris-HCl, pH 8.0) was purchased from Evrogen (Moscow, Russia). Gold chloride trihydrate ($HAuCl_4 \cdot 3H_2O$) and Tris-(2-carboxyethyl) phosphine hydrochloride (TCEP) were obtained from Aladdin Industrial Inc. Tris-HCl was obtained from Sigma-Aldrich (St. Louis, USA). 6-Mercapto-1-hexanol (MCH) was purchased from Adamas Reagent Co., Ltd.

Table 1. Sequences of oligonucleotides used in this work.

Name	Sequence (5′–3′)
P_{21}-Fc	Fc–TCAACATCAGTCTGATAAGCTA-SH-$(CH_2)_6$
P_{155}-MB	MB-ACCCCTATCACGATTAGCATTAA-SH-$(CH_2)_6$
miR-21 (T_1)	UAGCUUAUCAGACUGAUGUUGA
miR-155 (T_2)	UUAAUGCUAAUCGUGAUAGGGGU
miR-21-1 mis (SM1)	UAGCUUAUCAGACUGAUGUUCA
miR-21-3 mis (TM1)	UAGCUUAUCAGACUCAUCUUCA
miR-155-1 mis (SM2)	UUAAUGCUAAUCGUGAUAGGGCU
miR-155-3 mis (TM2)	UUAAUGCUAAUCGUCAUACGGCU
miR-16	UAGCAGCACGUAAAUAUUGGCG
let-7a	UGAGGUAGUAGGUUGUAUAGUU

(Shanghai, China) and used as received. RNase inhibitor, 20 bp DNA ladder, and 10× loading buffer were purchased from TaKaRa Biotechnology Co., Ltd (Dalian, China). The tips and tubes used were also RNase free and did not require pretreatment to inactivate RNases. All reagents were of analytical grade and used as received without further purification.

2.2. Apparatus and Electrochemical Measurements

The morphologies and structures of the obtained electrodes were characterized using field-emission scanning electron microscopy (FESEM) and energy dispersive spectroscopy (EDS; JEOL-6300F). X-ray photoelectron spectroscopy (XPS) measurements were conducted by a 5300 ESCA instrument. RT-qPCRs were performed using a Bio-Rad CFX96 thermal cycler, which was also used to analyze the reaction products (BIORAD, America). Cyclic voltammetry (CV), electrochemical impedance spectroscopy (EIS), square wave voltammetry (SWV), and other electrochemical measurements were performed using CHI 760E electrochemical workstation (Shanghai CH Instrument, China) with a conventional three electrode system (reference electrode: Ag/AgCl (3 M KCl), counter electrode: platinum wire, working electrode: the prepared CP-based electrode). CV scanning potential varied from –0.2 to +0.6 V, and the quiet time, scan rates ,and sample interval were 2 s, 50 mV s^{-1}, and 1 mV, respectively. EIS investigation was performed with the frequencies ranging from 10^{-1} to 10^5 Hz. SWV measurements were carried out by scanning from –0.6 to +0.6 V at amplitude of 25 mV and frequency of 15 Hz.

2.3. Preparation of CP/GNAs/AuNPs Electrode

Radio frequency plasma-enhanced chemical vapor deposition (RF-PECVD) system was employed to deposit GNAs onto clean carbon paper (CP) substrates. Briefly, 5 cm × 5 cm carbon paper was washed in acetone for 5 min, then rinsed with deionized water and dried for use. Then, the CPs were heated up to 750 °C by the furnace and cleaned with H_2 plasma for 30 min. Subsequently, a mixture of gases methane (CH_4) and hydrogen (H_2) with typically flow ratio of 2:3 was used to grow GNAs by the PECVD method, the substrates were heated up at 750 °C for 60 min under system pressure (P) of 40 Pa, with a power of 200 W. After growth, the CPs were removed from the furnace and cooled to room temperature under high vacuum conditions. The as-prepared CP/GNAs was cut to 0.7 cm × 0.7 cm, and it was immersed in 2 mM $HAuCl_4$ solution containing 0.01 M H_2SO_4 and Na_2SO_4 (v/v = 1:1) through i–t technique at a potential of –0.2 V for 200 s for the electrodeposition of AuNPs.

2.4. DSN-Assisted Target Recycling

For the DSN-assisted target recycling, the as-prepared CP/GNAs/AuNPs electrodes were immersed in 0.5 mL 1 × TM buffer (3 mM TCEP) containing 0.4 μM of P_{21}-Fc and P_{155}-MB and incubated for 2 h at 37 °C condition via Au–S bonding. Then, the electrodes were rinsed several times with PBS, the resulting electrodes surface were blocked with 2 mM MCH solution for 15 min and rinsed with DI water. Add 5 μL of RNase inhibitor (10 U μL^{-1}), 2 μL of DSN (0.5 U μL^{-1}), and different concentrations of the target miRNAs into 5 mL 0.01 M PBS to perform DSN-assisted target recycling at 50 °C.

2.5. Clinical Sample Detection and Methodology Comparison

In total, 18 clinical blood samples were collected from individuals at Chongqing University Cancer Hospital. Among these samples, six samples were from lung cancer inpatients, six samples were from breast cancer inpatients, another six samples from healthy individuals were selected as controls. This study was approved by the Ethics Committee of the Chongqing Cancer Hospital and performed in accordance with the Declaration of Helsinki and the International Ethical Guidelines for Biomedical Research Involving Human Subjects. Consent to exempt informed consent. This study is exempt from collecting informed consent. In order to protect the privacy of patients, patients' names, ID Numbers and mobile phone numbers were not collected during the experiments. All peripheral venous blood samples were collected in BD Vacutainer tubes (Franklin Lakes, NJ) and then centrifuged at 1500 rpm for 20 min. The plasma was immediately separated, frozen, and stored at –80 °C until detection and analysis, with no freeze–thaw cycles. The plasma was then divided into two equal parts for detection using the proposed CP/GNAs/AuNPs platform or qRT-PCR. The 1 mL plasma sample and 4 mL of PBS were mixed into test solution and detected by the proposed CP/GNAs/AuNPs platform.

Total miRNA was extracted from the plasma using miRNA extract reagent (Sangon, China) according to the manufacturer's protocol. Concentrations of isolated miRNA were quantified using a BioMate 3S spectrophotometer (Thermo Scientific, USA). The pure and concentrated miRNA was detected using qRT-PCR. To deactivate or solubilize proteins that might inhibit qRT-PCR, 2.5 μL of each plasma sample was mixed with 2.5 μL of a preparation buffer containing 2.5% Tween 20, 50 mmol L^{-1} Tris, and 1 mmol L^{-1} EDTA. The miRNA was reverse-transcribed into cDNA using an RT kit (Sangon, China) by a stem loop-mediated method. The transcribed cDNA was then used as the template for qPCR using a 2× SG Fast qPCR Master Mix kit (BBI, China).

All values were presented as the mean ± standard deviations of independent experiments. The results were analyzed by an unpaired, two-tailed Student's t test (two groups) or ANOVA (three or more groups) followed by Bonferroni's correction if needed. All of the statistical tests were performed with GraphPad Prism software version 8.0, and $p < 0.05$ was considered statistically significant.

3. Results and Discussion

3.1. Design of the GNAs/AuNPs DNA-Circuit Strip

Scheme 1 schematically illustrates the procedure of the fabricated of GNAs/AuNPs DNA-circuit strip and the detail process of miR-21 dynamic quantitative monitoring. As shown in Scheme 1A, graphene sheets were vertically grown on the CP to

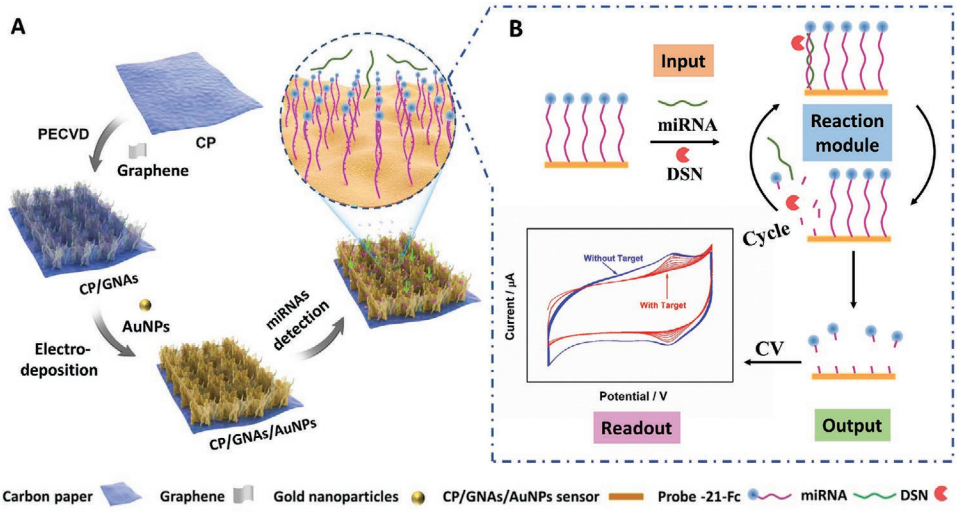

Scheme 1. A) Schematic representation of the process of disposable 3D GNAs/AuNPs DNA-circuit strip for miRNAs dynamic quantification using B) DSN-assisted signal amplification.

build 3D, continuous, and dense graphene nanoarrays (GNAs). Then, AuNPs were electrodeposited on both the layers and skeleton of the GNAs to form CP/GNAs/AuNPs electrode, which demonstrates a super-large surface area, by which ample biomolecular probes could be sufficiently immobilized. Scheme 1B shows that the DNAase-triggered assay quantifies the original target concentration by capturing the linearly amplified raw electrochemical signal from the target miRNAs. The ssDNA probe modified by electroactive material (ferrocene [Fc]), which acts as electrochemical signal reporter, is immobilized on the CP/GNAs/AuNPs electrode through the Au–S-based conjugation. In the presence of target miRNA (act as a powerful switch), the thiolated ssDNA probe hybridizes to the target to form a miRNA-DNA hybrid, which in turn serves as a substrate for DSN hydrolyze. Since the DSN only hydrolyzes the ssDNA oligonucleotide in a miRNA-DNA duplex, the target miRNA could be released upon cleavage and rehybridize to the remaining ssDNA probe, initiating another round of cleavage, release, and hybridization. In a system with sufficient DSN, the target miRNA and DSN would react repeatedly, allowing for a linear amplification of the redox peak shift signal in real time until all of the immobilized ssDNA probes have been cleaved.

3.2. Characterization of CP/GNAs/AuNPs Electrode

The surface morphology of the CP, CP/GNAs, and CP/GNAs/AuNPs were characterized by scanning electron microscopy (SEM). **Figure 1**B clearly shows that continuous 3D network structure of graphene sheets vertically erected on the smooth surface of carbon paper (CP) (Figure 1A) to form a compact GNA, greatly enlarging the specific surface area of the bare CP. As shown in Figure 1C, it is obviously observed that spherical AuNPs with the average size of ≈30 nm were electrodeposited on both the layers and skeleton of the GNAs. Furthermore, energy dispersive spectrometer (EDS) element mapping analysis displays that the prepared electrode only contains C and Au elements, which are homogeneously distributed (Figure 1D), suggesting successful preparation of the CP/GNAs/AuNPs electrode. In addition, Figure 1E,F exhibits images of the proposed electrodes with unique advantages, such as flexible, easy to cut, light, and convenient, and we manipulated it into a 0.7×0.7 cm^2 square in this work.

XPS was used to further examine the chemical composition of the as-prepared CP/GNAs/AuNPs electrode. Figure S1A, Supporting Information exhibits distinct C 1s, Au 4f peaks for electrodes. Figure S1B, Supporting Information illustrates the high-resolution C1s XPS spectrum of the CP/GNAs/AuNPs, which is decomposed into two distinct curves with the peaks appearing at 284.4 and 285.1 eV, corresponding to the C sp^2 and C sp^3 bonds, respectively.[37,38] The high-resolution Au 4f spectra of the prepared electrodes are shown in Figure S1C, Supporting Information, Au 4f peaks were observed at binding energies of 84.13 and 87.78 eV, corresponding to Au $4f_{7/2}$ and $4f_{5/2}$, respectively.[37,39]

3.3. Electrochemical Properties of the GNAs/AuNPs DNA-Circuit Strip

Cyclic voltammetry (CV) and EIS were employed in 5 mM $[Fe(CN)_6]^{3-/4-}$ (1:1) solution containing 0.1 M KCl to investigated the electrochemical properties of the proposed GNAs/AuNPs DNA-circuit strip. **Figure 2**A shows the comparison of the CV responses for the bare CP (curve a), CP/GNAs (curve b), CP/GNAs/AuNPs (curve c), CP/GNAs/AuNPs/P_{21}-Fc (curve d), and CP/GNAs/AuNPs/P_{21}-Fc/miR-21+DSN (curve e). A pair of well-defined quasi-reversible redox peaks (Fe $^{2+/3+}$ redox couple) is observed on the bare CP (curve a), when the CP surface was vertically grown with GNAs (curve b), both anodic and cathodic peak currents obviously increase, indicating that GNAs can enhance the electron transfer kinetics due to its superior conductivity.[40] As expected, the redox peak currents are further increased after the AuNPs were electrodeposited on the CP/GNAs (curve c). The peaks current decreased dramatically after immobilization of P_{21}-Fc on the CP/GNAs/AuNPs via

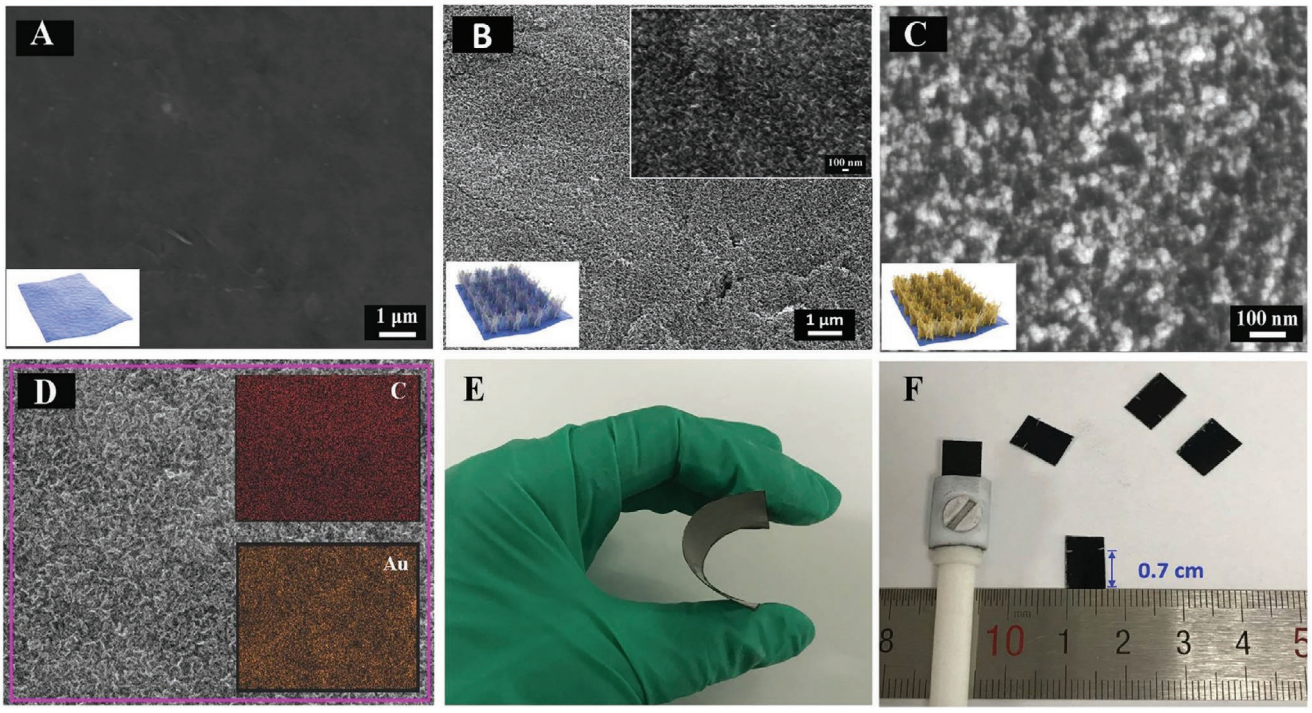

Figure 1. SEM images of A) bare carbon paper (CP), B) carbon paper/graphene nanoarrays (CP/GNAs), C) carbon paper/graphene nanoarrays/gold nanoparticles (CP/GNAs/AuNPs), and D) EDS element mapping of CP/GNAs/AuNPs. Images of the prepared E) CP/GNAs (5 × 5 cm^2) and F) CP/GNAs/AuNPs with a size of 0.7 × 0.7 cm^2.

Au–S bond (curve d), which might be ascribed the electrostatic repulsion between the negatively charged thiolated P_{21}-Fc and $[Fe(CN)_6]^{3-/4-}$.[41] In contrast, when the mixture solution (10 nM target miR-21 and DSN) was added, forming miRNA:DNA heteroduplexes that can be hydrolyzed by DSN. The immobilized P_{21}-Fcs were gradually cleaved and then a distinct recovery in current peaks (curve e), confirming the successful fabrication of the developed miRNA biosensor.[42]

EIS is an effective and convenient method for investigating the surface features of the surface-modified electrodes. As shown in Figure 2B, the electron transfer resistance (R_{et}) decreases successively with the modification of GNAs (curve b) and GNAs/AuNPs (curve c). When P_{21}-Fc immobilized on the CP/GNAs/AuNPs and the value of *R*ct greatly increased (curve d), then the *R*ct decreased after the miRNA and DSN addition (curve e), which were consistent with the changes observed in CVs. Both CV and EIS results indicate that GNAs/AuNPs enlarged electroactive surface area because of the porous 3D-networked nanostructure, good electrical conductivity of GNAs/AuNPs, and well-distributed AuNPs, which is beneficial for the immobilization of biomolecules probes and improvement of the sensitivity of the biosensor.

3.4. Dynamic Quantitative Monitoring of miR-21

miR-21 was selected as the model to demonstrate the proposed GNAs/AuNPs DNA-circuit strip because this miRNA is

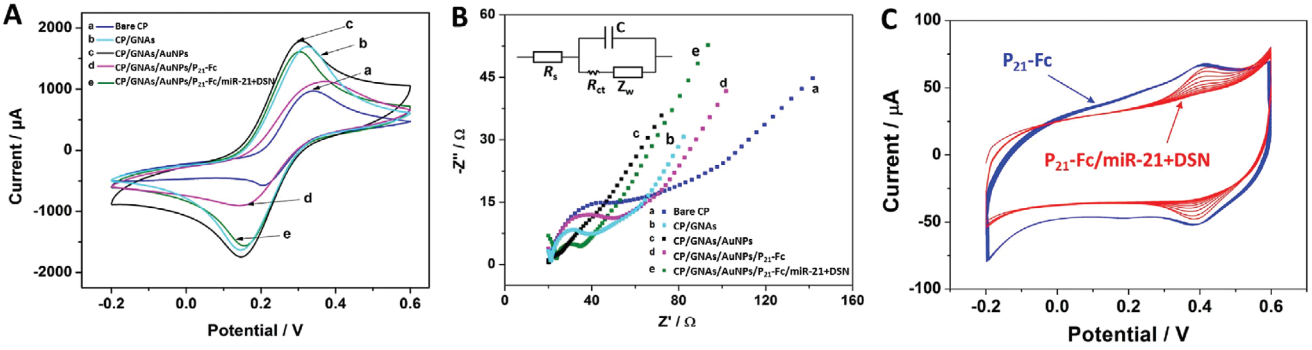

Figure 2. A) CVs and B) EISs obtained for bare CP (a), CP/GNAs (b), CP/GNAs/AuNPs (c), CP/GNAs/AuNPs/P_{21}-Fc (d), and CP/GNAs/AuNPs/P_{21}-Fc/miR-21+DSN (e) in 5 mM $[Fe(CN)_6]^{3-/4-}$ (1:1) solution containing 0.1 M KCl. C) The CV curves obtained for CP/GNAs/AuNPs/P_{21}-Fc (blue curve) and CP/GNAs/AuNPs/P_{21}-Fc/miR-21+DSN (red curve) in 0.01 M PBS solution (taking a circle of CV curve every 2 min of the original CV curves), scan rate is 50 mV s^{-1}.

a prevalent cmiRNA biomarker that is overexpressed in various human cancers.[43] An ssDNA probe (P_{21}-Fc) complementary to miR-21 (10 nM) was prepared and immobilized on the CP/GNAs/AuNPs electrode surface exhibits a sharp Fc redox peak at 0.38 V was scanned through cyclic voltammetry (CV) with 200 cycles (Figure S2, Supporting Information, blue curve). The signal amplification process could be monitored continuously as the number of hybridization-cleavage cycles increased. In the presence of both the target miR-21 and DSN, the Fc redox peak gradually decreased until reaching an end point. When the miRNA–DNA hybrid is completely formed; the ongoing hybridization-cleavage step will then induce a gradual decrease in the Fc redox peak until the end of the stage, at which point all the coated probes have been cleaved (Figure S2, Supporting Information, red curve). In order to make it clearer for us to observe the dynamic enzymatic digestion process, we selected a CV curve every 2 min of the original CV curves for analysis (Figure 2C). In addition, the DSN-mediated cleavage of the ssDNA in the miRNA–DNA hybrid was further confirmed by 12% polyacrylamide gel electrophoresis (PAGE). As seen in Figure S3, Supporting Information, the target miR-21 (lane 2), DNA probe 21 (SH-P_{21}-Fc) (lane 3), and the miRNA-DNA hybrid (lane 4) could be obviously observed without the DSN enzyme. However, there were only miR-21 shallow band in the DSN-cleaved product (lane 5), verifying the successful hydrolysis of the DNA in the miRNA–DNA complex.

To further optimize the prepared CP/GNAs/AuNPs electrode for miRNA detection, the P_{21}-Fc concentration and the incubation time of P_{21}-Fc were selectively optimized. During the process of optimizing any one parameter, all other parameters are maintained at their optimal conditions. First, the sensitivity of this developed miRNA sensor depends on the amount of immobilized P_{21}-Fc. In the range from 0.2 to 1 μM, Figure S4A, Supporting Information shows that increasing concentration of P_{21}-Fc leads to increased current response of Fc, reaching a maximum peak value at 0.6 μM, and then the current response remained stable thereafter. Besides, the incubation time of P_{21}-Fc is another parameter with significant impact on the performance of the sensor. As shown in Figure S4B, Supporting Information, the current signal of P_{21}-Fc initially increases almost linearly within 2 h and then leveled off thereafter. Thus, 0.6 μM P_{21}-Fc and 2 h incubation time were chosen in the subsequent experiments.

As shown in **Figure 3**A–E, the dynamic characteristics for miR-21 sensing were investigated, a series of concentrations (10 fM, 100 fM, 1 pM, 10 pM, and 100 pM) were employed to reflect the DNAase-triggered assay. We observed that the entire hybridization-cleavage process was investigated within 20 min under optimal conditions, suggesting a near end of the process. As shown in Figure 3F, the shift of Fc redox peak signals decreased quickly before 16 min, and the rates of shift increased with the increase of target miRNA concentration. The shift of Fc redox peak signals growth slowed down gradually when the time reached 20 min. Thus, we chose 16 min as the optimal reaction time. These results illustrate that the target miRNA concentration could be determined dynamically by plotting the target concentration against the shift of Fc redox peak signal.

3.5. Dual-Target Detection of miR-155 and miR-21

To achieve better analytical performance of the developed miRNA sensor in two or multiple detections, an ssDNA probe-modified methylene blue (P_{155}-MB) complementary to miR-

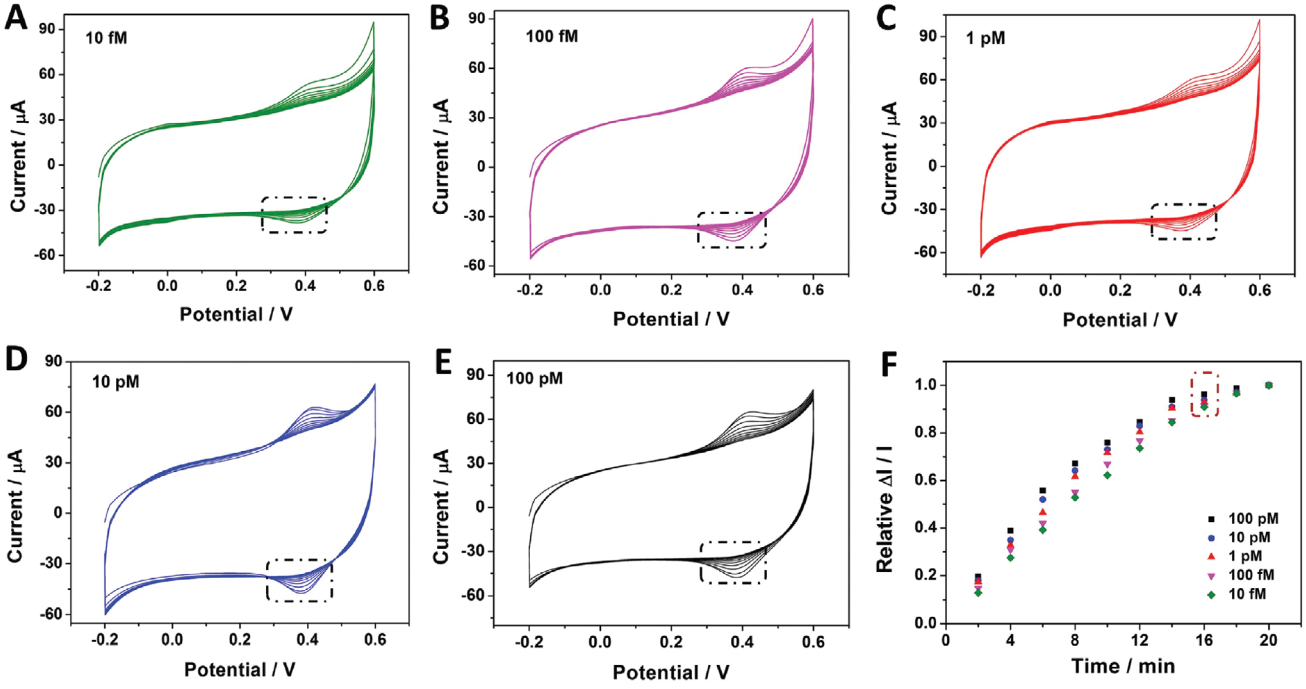

Figure 3. Dynamic monitoring by CV of miR-21: A) 10 fM, B) 100 fM, C) 1 pM, D) 10 pM, and E) 100 pM, taking a circle of CV curves every 2 min, scan rate is 50 mV s^{-1}. F) The corresponding calibration curve for time of (A–E).

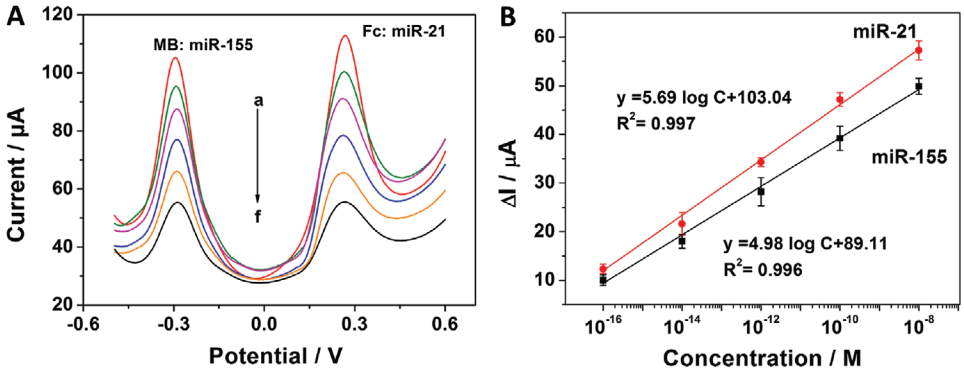

Figure 4. A) SWV responses for the detection of different concentrations of miR-21 and miR-155 with the proposed CP/GNAs/AuNPs sensor in 0.01 M PBS (pH = 7.4) (from a to f: 0 aM, 100 aM, 10 fM, 1 pM, 100 pM, and 10 nM). B) The corresponding calibration plots of (A). Error bars: SD, $n = 3$.

155 was employed as another model. In addition, SWV, an advanced electrochemical technique with fine background correction capability and high sensitivity, was employed for the simultaneous quantitative analysis of miR-155 and miR-21. Under the optimized conditions, we further investigated the performance of current peak signal upon different concentrations of miR-155 and miR-21. As illustrated in **Figure 4**A, the shifts of Fc peak and MB peak gradually increase with the elevated concentration of target miRNA. Figure 4B shows a great linear correlation between the redox peak shift and logarithm of miRNA concentration from 100 aM to 10 nM. The miR-155 correlation equation is $Y = 4.98 \log C + 89.11$, with a correlation coefficient $R^2 = 0.996$, and the miR-21 correlation equation is $Y = 5.69 \log C + 103.04$, with a correlation coefficient $R^2 = 0.997$, where Y is the ΔI (the value of peak current between I_0 and the one in the presence of miR-21), and C is the concentration of miRNA (M). The limits of detection (LOD) for miR-21 and miR-155 are calculated to be 21.4 and 30.3 aM (S/N = 3), respectively.

3.6. Specificity and Reproducibility of the Proposed miRNA Biosensor

To further investigate the selectivity of this sensor, interfering miRNAs including single-base mismatched (SM), three-base mismatched (TM), and unmatched miRNAs (miR-16, let-7a) were introduced. **Figure 5**A shows that only hybridized with the complementary (CM) targets (10 nM miR-155 and miR-21), the peak current variation (ΔI) reached the maximum, and any mismatched targets produced negligible currents, indicating the high specificity of the proposed CP/GNAs/AuNPs electrode in discriminating short-stranded target miRNAs. To further investigate the reproducibility of this CP/GNAs/AuNPs electrode (Figure 5B), five electrodes with the same modification were fabricated in different batches to test trace miRNA with the same concentration (10 nM). We observed acceptable relative standard deviations (RSD) of 3.03% (miR-155) and 3.29% (miR-21), respectively, indicating that the proposed approach has satisfactory reproducibility.

3.7. Clinical Sample Detection and Methodology Comparison

To further determine the feasibility and reliability of this miRNA sensor in clinical samples, 18 clinical blood samples of patients with non-small cell lung cancer inpatients (6 samples), breast cancer inpatients (6 samples), and healthy individuals (6 samples as control) from Chongqing University Cancer Hospital (Chongqing, China) were determined using both the proposed CP/GNAs/AuNPs electrode and the classical qRT-PCR. Identical discrimination capabilities were observed between the two approaches (**Figure 6**A,B), showing that the abundances of miR-155 in blood of individuals are in the order of breast cancer > NSCLC patients > negative control,

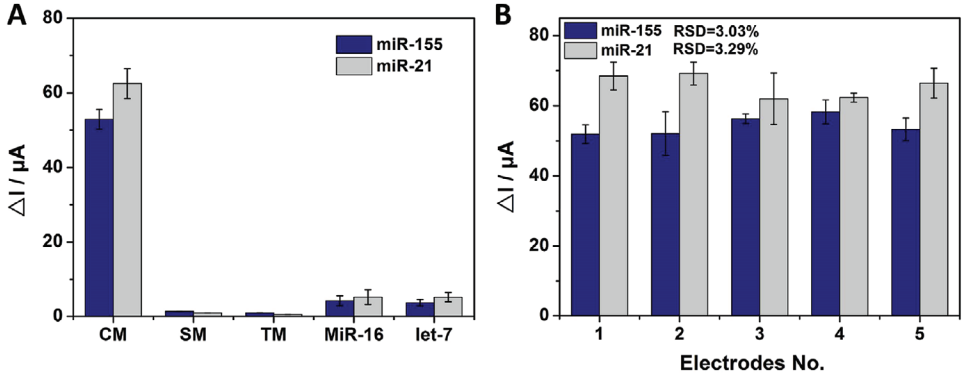

Figure 5. A) Specificity of the CP/GNAs/AuNPs sensor: complementary match (CM), single-base mismatch (SM), three-base mismatch (TM), miR-16, and let-7a. B) Reproducibility of the proposed miRNA biosensor. The error bars indicate standard deviations from five measurements ($n = 5$).

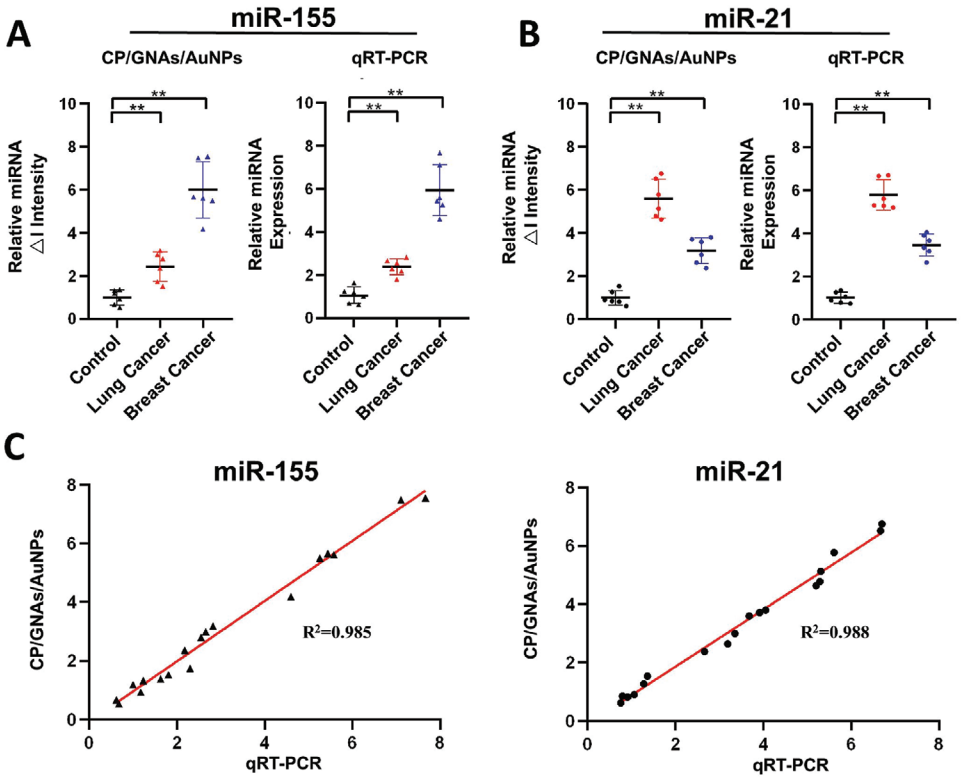

Figure 6. A,B) Validation of clinically differentiating lung cancer (red) and breast cancer (blue) from normal sample (black) using miR-155 (triangle) and miR-21 (dot). Error bars: SD, $n = 3$. C) Fitting curves of regression analysis of CP/GNAs/AuNPs sensor and qRT-PCR in detecting miRNA-155 and miRNA-21.

whilst the abundances of miR-21 are in the order of NSCLC patients > breast cancer patients > negative control, which is similar to those results in the literature.[1,44] Moreover, Figure 6C demonstrated a good correlation between the proposed method and qRT-PCR for detecting the two molecules (miR-155 $R^2 = 0.958$, $p < 0.0001$; miR-21 $R^2 = 0.988$, $p < 0.0001$). We observed the miR-155 and miR-21 concentrations in the control group were significantly lower than which in these cancer patients, suggesting that the proposed assay can effectively quantify circulating miRNAs in various cancers, indicating that the CP/GNAs/AuNPs sensor represents a promising method for clinical applications.

4. Conclusion

In summary, we developed a sensitive and selective 3D GNAs/AuNPs DNA-circuit strip for dynamic quantitative monitoring of miRNAs. GNAs can be vertically and controllably tethered in situ by RF-PECVD, CP/GNAs/AuNPs sensor shows a huge specific surface area and can expose more active sites, thus greatly improving the immobilization of probes and increasing molecular hybridization efficiency. In addition, the dynamic detection of cancer-related miRNAs was achieved. The developed biosensor achieved the dynamic quantitative monitoring of miRNAs with different concentrations, and shows a linear detection range of 100 aM to 10 nM for cancer-related miRNAs with detection limits of 21.4 and 30.3 aM (time: 16 min) for the simultaneously determination of miR-21 and miR-155, respectively. Importantly, the sensor offers high analytical performance in terms of selectivity, reproducibility, and stability, and also shows good application with qRT-PCR in clinical detection analysis of miRNAs, suggesting that the developed DNA-circuit strip could be used for other cancer-related biomolecules. Therefore, the proposed disposable GNAs/AuNPs DNA-circuit strip is sensitive, portable, disposable, and convenient, exhibiting a promising potential in early cancer prevention and rapid detection platforms for point-of-care clinical analysis.

Supporting Information

Supporting Information is available from the Wiley Online Library or from the author.

Acknowledgements

J.B., X.Q., and H.Y. contributed equally to this work. This work was supported by the National Natural Science Foundation of China (81772290, 81601854, and 81871733); the Graduate Research and Innovation Foundation of Chongqing, China (CYB17037); Chongqing science and technology commission (CSTC2018jcyjAX0062); the Fundamental Research Funds for the Central Universities (2019CDYGZD007, 2019CDYGZD005); Chongqing Graduate Tutor Team Construction Project and Analytical and Testing Center of Chongqing University for SEM and the sharing fund of Chongqing University's large equipment.

Conflict of Interest

The authors declare no conflict of interest.

Keywords

DNA-circuit strips, duplex-specific nuclease enzyme, dynamic quantification, graphene nanoarrays, microRNAs

Received: March 4, 2020
Revised: June 2, 2020
Published online:

[1] H. Dong, J. Lei, L. Ding, Y. Wen, H. Ju, X. Zhang, *Chem. Rev.* **2013**, *113*, 6207.
[2] L. Inhan, S. S. Ajay, C. Haiming, M. Atsushi, W. Nulang, M. G. McInnis, B. D. Athey, *Nucleic Acids Res.* **2008**, *36*, e27.
[3] J. U. Lee, W. H. Kim, H. S. Lee, K. H. Park, S. J. Sim, *Small* **2019**, *15*, 1804968.
[4] J. Liu, Y. Wen, H. He, H. Y. Chen, Z. Liu, *Chem. Sci.* **2018**, *9*, 7241.
[5] F. Xu, H. Dong, Y. Cao, H. Lu, X. Meng, W. Dai, X. Zhang, K. A. Al-Ghanim, S. Mahboob, *ACS Appl. Mater. Interfaces* **2016**, *8*, 33499.
[6] T. Kilic, A. Erdem, M. Ozsoz, S. Carrara, *Biosens. Bioelectron.* **2017**, *99*, 525.
[7] G. S. Pall, C. Codonyservat, J. Byrne, L. Ritchie, A. Hamilton, *Nucleic Acids Res.* **2017**, *35*, e60.
[8] H. Willenbrock, J. Salomon, R. Søkilde, K. B. Barken, T. N. Hansen, F. C. Nielsen, S. Møller, T. Litman, *RNA* **2009**, *15*, 2028.
[9] M. Steinau, M. S. Rajeevan, E. R. Unger, *J. Mol. Diagn.* **2006**, *8*, 113.
[10] X. Qiu, H. Zhang, H. Yu, T. Jiang, Y. Luo, *Trends Biotechnol.* **2015**, *33*, 180.
[11] D. A. Shagin, D. V. Rebrikov, V. B. Kozhemyako, I. M. Altshuler, A. S. Shcheglov, P. A. Zhulidov, E. A. Bogdanova, D. B. Staroverov, V. A. Rasskazov, S. Lukyanov, *Genome Res.* **2002**, *12*, 1935.
[12] Q. Xiaopei, L. Xing, Z. Wei, Z. Hong, J. Tianlun, F. Dongli, L. Yang, *Anal. Chem.* **2015**, *87*, 6303.
[13] B. C. Yin, Y. Q. Liu, B. C. Ye, *J. Am. Chem. Soc.* **2012**, *134*, 5064.
[14] Y. Ren, H. Deng, W. Shen, Z. Gao, *Anal. Chem.* **2013**, *85*, 4784.
[15] F. Causa, A. Aliberti, A. M. Cusano, E. Battista, P. A. Netti, *J. Am. Chem. Soc.* **2015**, *137*, 1758.
[16] H. Liao, Y. Zhou, Y. Chai, R. Yuan, *Biosens. Bioelectron.* **2018**, *114*, 10.
[17] G. Maduraiveeran, M. Sasidharan, V. Ganesan, *Biosens. Bioelectron.* **2017**, *103*, 113.
[18] S. Su, Y. Wu, D. Zhu, J. Chao, X. Liu, Y. Wan, Y. Su, X. Zuo, C. Fan, L. Wang, *Small* **2016**, *12*, 3794.
[19] J. Das, I. Ivanov, T. S. Safaei, E. H. Sargent, S. O. Kelley, *Angew. Chem.* **2018**, *130*, 3773.
[20] W. Nongnoot, S. Marcel, G. Christian, J. B. Antje, *Chem. Rev.* **2019**, *119*, 120.
[21] F. Xiao, L. Wang, H. Duan, *Biotechnol. Adv.* **2016**, *34*, 234.
[22] Z. Farka, T. Juřík, D. Ková, L. Trnková, P. Skládal, *Chem. Rev.* **2017**, *117*, 9973.
[23] Y. Han, Z. Qiu, G. N. Nawale, O. P. Varghese, J. Hilborn, B. Tian, K. Leifer, *Biosens. Bioelectron.* **2018**, *127*, 188.
[24] V. K. Singh, S. Kumar, S. K. Pandey, S. Srivastava, A. Srivastava, *Biosens. Bioelectron.* **2018**, *105*, 173.
[25] A. Ghosale, K. Shrivas, R. Shankar, V. Ganesan, *Anal. Chem.* **2017**, *89*, 776.
[26] C. P. Lee, K. Y. Lai, C. A. Lin, C. T. Li, K. C. Ho, C. Wu, S. P. Lau, J. H. He, *Nano Energy* **2017**, *36*, 260.
[27] W. Dungchai, O. Chailapakul, C. S. Henry, *Anal. Chem.* **2009**, *81*, 5821.
[28] M. K. Chuang, S. W. Lin, F. C. Chen, C. W. Chu, C. S. Hsu, *Nanoscale* **2014**, *6*, 1573.
[29] H. Y. Mao, S. Laurent, W. Chen, O. Akhavan, M. Imani, A. A. Ashkarran, M. Mahmoudi, *Chem. Rev.* **2013**, *113*, 3407.
[30] H. Yenny, N. Valeria, L. Mustafa, M. Fiona, B., S. Zhenyu, D. Sukanta, T. I., M., H. Brendan, B. Michele, K. Yurii, G. K., J. John, B., N. Peter, D. Georg, K. Satheesh, G. Robbie, H. John, S. Vittorio, C. F. Andrea, *Nat. Nanotechnol.* **2008**, *3*, 563.
[31] C. Y. Su, A.-Y. Lu, Y. Xu, F.-R. Chen, A. N. Khlobystov, L.-J. Li, *ACS Nano* **2011**, *5*, 2332.
[32] A. Ambrosi, M. Pumera, *Nanoscale* **2013**, *6*, 472.
[33] P. W. Sutter, J.-I. Flege, E. A. Sutter, *Nat. Mater.* **2008**, *7*, 406.
[34] P. Li, Z. Jin, L. Peng, F. Zhao, D. Xiao, Y. Jin, G. Yu, *Adv. Mater.* **2018**, *30*, 1800124.
[35] Y. Ma, W. Jiang, J. Han, Z. Tong, M. Wang, J. Suhr, X. Chen, L. Xiao, S. Jia, H. Chae, *ACS Appl. Mater. Interfaces* **2019**, *11*, 10237.
[36] V. P. Pham, H.-S. Jang, D. Whang, J.-Y. Choi, *Chem. Soc. Rev.* **2017**, *46*, 6276.
[37] S. Bo, J. Zhao, M. Wang, J. Mullavey, Y. Zhu, Z. Geng, D. Chen, D. Yong, K. S. Moon, M. Liu, *Nano Energy* **2017**, *31*, 183.
[38] J. H. Lin, H. N. Jia, Y. F. Cai, L. C. Shu, W. D. Fei, *J. Mater. Chem. A* **2017**, *6*, 908.
[39] H. Fu-An, F. Jin-Tu, S. Fei, Z. Li-Ming, L. W. C. Helen, *Nanoscale* **2011**, *3*, 1182.
[40] C. Da, F. Hongbin, L. Jinghong, *Chem. Rev.* **2012**, *112*, 6027.
[41] C. Mei, C. Hou, D. Huo, B. Jing, H. Fa, C. Shen, *Biosens. Bioelectron.* **2016**, *85*, 684.
[42] R. Yuqian, D. Huimin, S. Wei, G. Zhiqiang, *Anal. Chem.* **2013**, *85*, 4784.
[43] J. Zhang, L. L. Wang, M. F. Hou, Y. K. Xia, W. H. He, A. Yan, Y. P. Weng, L. P. Zeng, J. H. Chen, *Biosens. Bioelectron.* **2017**, *102*, 33.
[44] B. Gloria, C. Claudia, C. Isabella, *Theranostics* **2015**, *5*, 1122.